

# Mechanical property improvement of quenchable steel by grinding

I. ZARUDI, L. C. ZHANG\*

*School of Aerospace, Mechanical and Mechatronic Engineering,  
The University of Sydney, NSW 2006, Australia  
E-mail: zhang@mech.eng.usyd.edu.au*

This paper studies a method of surface heat treatment by making use of grinding heat and stress to create favorable microstructures and promote high wear and fatigue resistance. It was found that the thickness of the treated surface layer could be up to 600  $\mu\text{m}$ . The beneficial microstructure of the layer was created by an enhanced martensite transformation, intensive dislocations and a more desirable carbon distribution. It is highly possible that the method can be used to incorporate grinding and surface hardening into a single grinding operation to develop a cost-effective production method.

© 2002 Kluwer Academic Publishers

## 1. Introduction

In the current manufacturing practice, elements after a soft machining need to be transported to the surface hardening bay, cleaned and undergone the heat treatment. They are then discharged, moved back and incorporated into the production line for a final precision surface finishing. The above process is time consuming and costly, but because of the characteristics of the existing techniques of heat treatment, it has been impossible to integrate a heat treatment process into a production line of surface finishing.

On the other hand, the thermo-mechanical process in surface finishing often brings about undesirable changes of the mechanical properties generated by heat treatment. For example, the material removal in grinding produces considerable amount of heat, and most heat conducts into the workpiece and often causes thermal damage. As a result, relevant studies on grinding technology in the last three decades have been trying to eliminate such damages by extracting the grinding heat from workpiece [1–3].

The above production procedure is inefficient because it wastes most grinding energy and makes the prevention of the treated surface structure difficult.

In the investigation on grinding-induced residual stresses in steel workpiece, Zhang and co-workers [4–6] found that phase transformation during surface grinding, which results in hardening characteristics, could be achieved by a proper selection of grinding conditions. Under the specified distribution of heat flux, convection process of coolants and constitutive models of workmaterials, the depth and nature of the martensitic layer and distribution of residual stresses can be described quantitatively with respect to the material removal rate and coolant application method.

Experimental studies [7, 8] also reported that the grinding energy could be used to generate hard surface layer and the term “grind-hardening” was introduced [7]. However, a hardened layer does not necessarily mean beneficial, rather, it can be very harmful if the layer is associated with a poor microstructure [1–3].

The purpose of the present work is to explore the thermo-mechanical mechanism of surface heat treatment by grinding and find out a reliable method for creating suitable functional properties of the ground component with high wear and fatigue resistance.

## 2. Experiment

The testing material selected was widely used steel, AISI 4140, initially tempered. The chemical composition of the steel is listed in Table I. To compare the material properties of the grinding-induced surface layer with those from a conventional heat treatment, the microstructure generated by standard quenching—heating a specimen to 850°C and quenching vigorously in oil—was also investigated.

Grinding was performed on a surface grinder, Minini Junior 90 CF CNC M286, with alumina grinding wheel. The grinding parameters as defined in Ref. [9] are listed in Tables II to III. Compressed air was used as coolant.

The material's hardness was examined on cross-section view samples by means of a conventional Micro-Hardness Tester (Type M of Shimadzu Seisakusho) and the properties of the ground surfaces were explored by a scanning electron microscope (SEM) 505 (JEOL). The characterization of the subsurface structure of the ground surfaces was done on a transmission electron microscope (TEM), CM12 (Philips), while the segregation of different elements

\*Author to whom all correspondence should be addressed.

TABLE I Chemical composition of the AISI 4140 steel

Chemical element	Fe	C	Si	Mn	Cr	Mo
%	Balance	0.40	0.25	0.80	0.90	0.20

TABLE II Grinding conditions

Workpiece material	Steel 4140
Grinding wheel	BWA120MVAA
Wheel diameter (mm)	280
Wheel speed (m/s)	27
Grinding width (mm)	15
Table speed (m/min)	0.1–5
Depth of cut ( $\mu\text{m}$ )	20–70
Coolant	Compressed air

TABLE III Wheel dressing conditions

Type of dresser	Single-point diamond
Wheel speed (m/min)	10
Dressing, cross-feed rate (mm/revolution)	0.1

were investigated on TEM Biofilter (Philips) using EELS mapping. Both plan- and cross-section view samples were used in the analysis. In sample preparation, the temperature throughout a specimen was kept below 40°C to ensure that no micro-structural changes took place.

Dry wear tests were carried out on a Plint-Cameron pin-on-disc machine. As illustrated in Fig. 1a, two pin samples were held against a rotating high-speed steel disc of hardness  $H_{MV} = 720$ . A fixed track diameter of 80 mm was used in all the tests. However, each test was run on a fresh track, with a sliding distance of

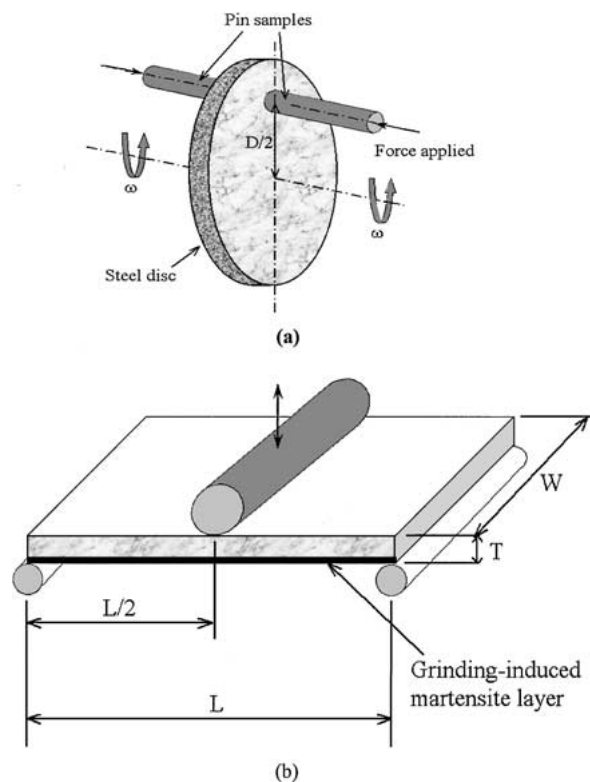


Figure 1 The schematic diagrams of property testing (a) pin-on-disc wear test; (b) fatigue test via three-point bending.

500 m, normal stress between 1 MPa and 5 MPa and sliding velocity of 0.98 m/s. Friction and wear results were taken from eight repeated tests under nominally identical sliding conditions. A transducer attached to the specimen holder recorded the tangential force. The volumetric wear was measured by the weight losses of the specimens using an analytical balance with resolution of 0.1 mg.

The fatigue experiments, using three-point bending as illustrated in Fig. 1b, were carried out on an alternating bending machine “Servopulser” (Shimadzu Seisakusho Ltd.) at 10 Hz. Flat samples with a gauge length of 20 mm and a cross-section of  $2 \times 15$  mm were used. Minimum replication level for the experiments was 80%.

### 3. Observation

For convenience of the discussion below, we will call the martensite introduced by the conventional quenching the *ordinary martensite* (OM) and the hardened layer generated by grinding the *grinding-induced layer* (GIL).

#### 3.1. Microstructure by optical microscopy

The optical micrographs of the OM and GIL are shown in Fig. 2. The ordinary martensite is characterized by a plate-like structure as revealed by etching in Fig. 2a. The depth of the GIL changes from 200  $\mu\text{m}$  (for the grinding conditions with the depth of cut 20  $\mu\text{m}$ ) to 600  $\mu\text{m}$  while grinding with the depth of cut of 70  $\mu\text{m}$  (Fig. 2b). The optical micrograph of the GIL is almost featureless, except certain inhomogeneity. However, some fine fragments can be seen in the immediate vicinity of the subsurface, whose size seems to increase towards the bottom of the layer. The properties of the layer will be discussed later.

#### 3.2. Micro-hardness

The micro-hardness across the GIL thickness can be seen in Fig. 3, which exceeds the original hardness of the steel ( $HV_{(300g)} = 350$ ) by 2.2 times and that of the OM ( $HV_{(300g)} = 560$ ) by 1.3 times. Minor fluctuations of hardness happened across the layer.

#### 3.3. Microstructure by electron microscopy

The microstructure of the OM observed using an electron microscope is shown in Fig. 4a. Martensite laths formed on quenching with crystals being grouped in packets. Areas with twinned martensite also appeared occasionally. The martensite crystals inside a packet were elongated in approximately the same direction, with an average length of 2–3  $\mu\text{m}$  and an average width of 0.3–0.5  $\mu\text{m}$ . The density of dislocations was high but carbides were not found.

In the GIL, however, the material of the first 5–6  $\mu\text{m}$  under the surface (Fig. 4b) was composed of fine and nearly circular grains with a characteristic dimension of 0.2–0.5  $\mu\text{m}$ . The  $c/a$  parameter of the structure, according to TEM, was in the range of 1.02–1.03, indicating that the structure was a martensite with a great refinement of grains. Moreover, the dislocation structure of the martensite fragments was mainly cellular, although

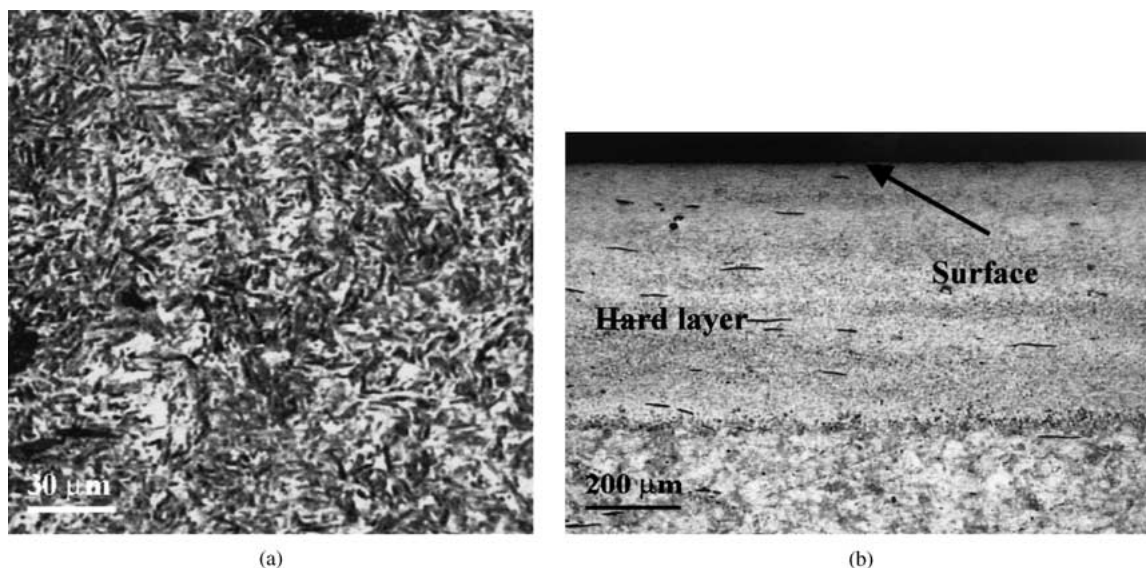


Figure 2 The structure under optical microscopy. (a) the ordinary martensite; (b) the grinding-induced layer (depth of cut = 70  $\mu\text{m}$ , table velocity = 0.1 m/min).

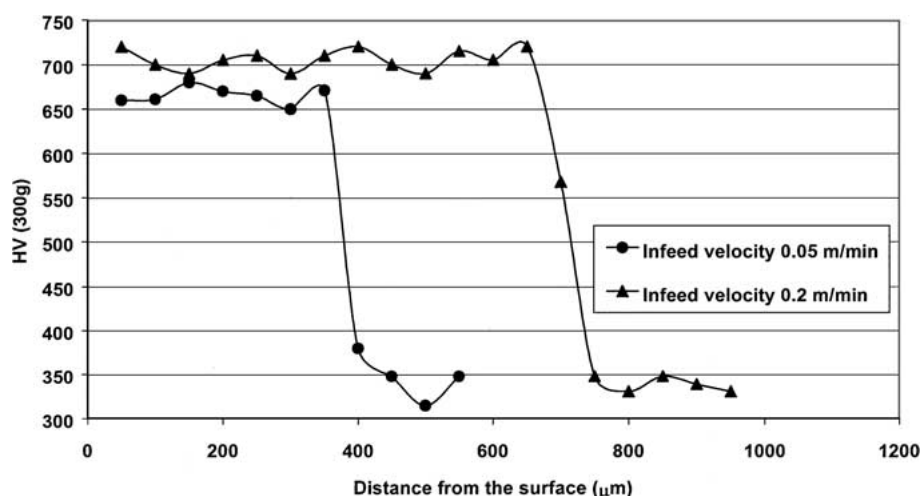


Figure 3 Effect of infeed velocity on micro-hardness of the grinding-induced layer (Depth of cut 70  $\mu\text{m}$ ).

polygonal regions occasionally appeared (Fig. 4c). No carbides were observed.

In the deeper subsurface of the GIL, martensite laths became greater. For example, at the depth of 200  $\mu\text{m}$  from the surface the characteristic dimension of the laths was 0.8–1  $\mu\text{m}$ . Again no carbides were admitted (Fig. 4d) and the dislocation structure of the sub-layer resembled that of the OM.

However, in the further deeper subsurface, at the depth of 400  $\mu\text{m}$  for instance (Fig. 4e), carbides could be easily located. There, the dislocation density was significantly lower.

### 3.4. Distribution of carbon

The distribution of carbon in GIL can be seen in Fig. 5, inhomogeneous in the top zone. Twinned martensite also appeared (Fig. 5a). The additional concentration of carbon in the twinned martensite fragments was found (Fig. 5b). It may be due to the fast formation of the layer. The table speed of grinding, as listed in Table II, indicates that the time of reaching the critical phase transformation temperature at a point near the surface is 1.4 s, which is not long enough to achieve a uniform

carbon distribution after the dissolution of carbides. As a result, areas with the high carbon content promoted the transformation to twinned martensite upon cooling. Segregations of carbon reached 6 nm (Fig. 5c and d) at the boundaries of martensite laths and 4 nm at dislocations (Fig. 9e and f).

In contrast with the GIL, no obvious inhomogeneity was seen among different laths of the OM. This means that the soaking time of 1 hour used in the ordinary quenching procedure was sufficient to achieve the homogeneous carbon distribution, although carbon segregations could also be located at lath boundaries and dislocations.

As carbon is mainly segregated along martensite laths its distribution in GIL is more uniform due to refinement of martensite laths. At the depth of 400  $\mu\text{m}$  all carbon was located in carbides (Fig. 5g and h).

## 4. Discussion

### 4.1. Formation mechanism of the GIL

The above observation shows that the microstructures of the OM and GIL are rather dissimilar, and the microstructure in GIL varies along the depth of the layer.

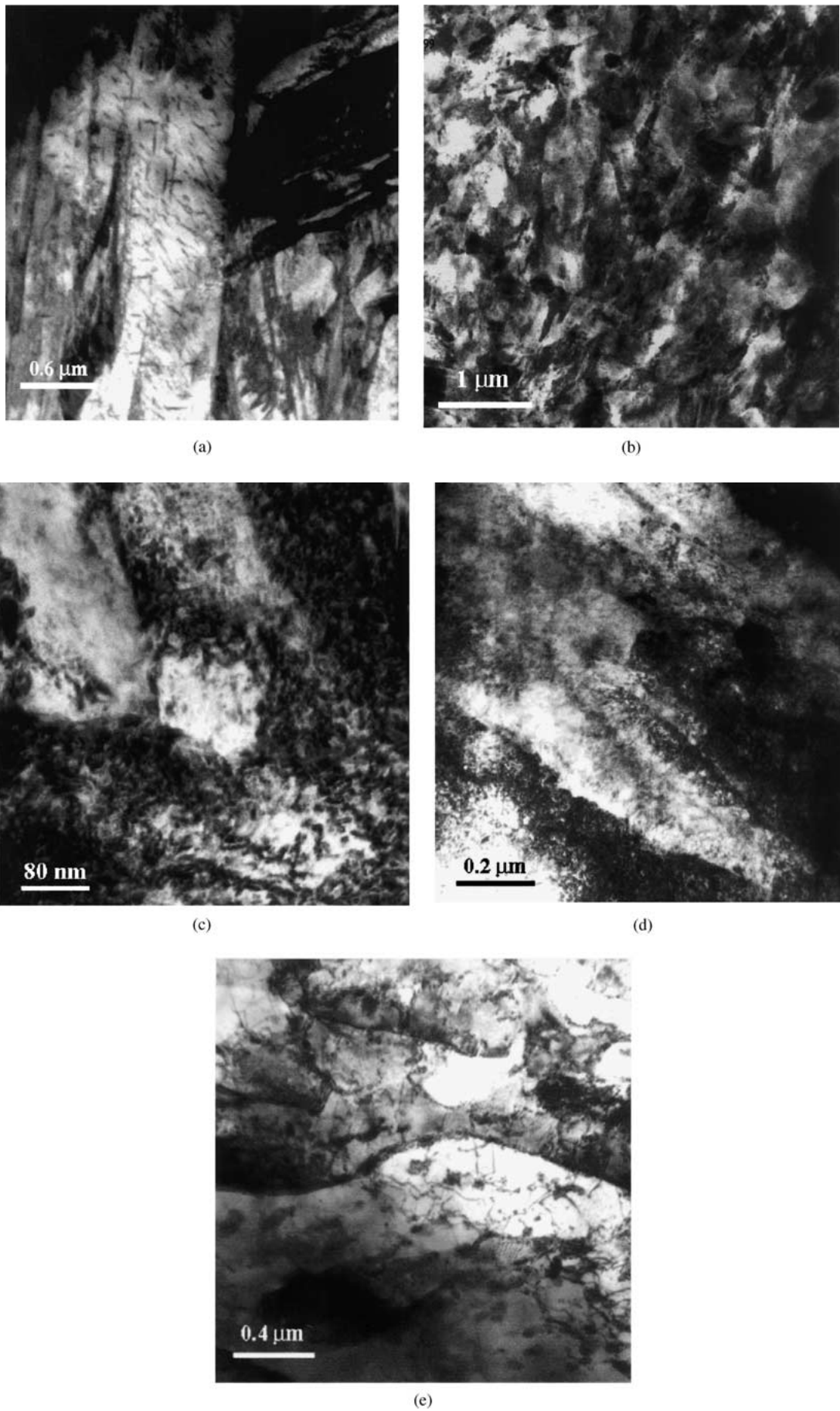


Figure 4 The structure under electron microscopy. (a) the OM. Note the large laths; (b) the top part of the GIL. Note the refined martensite laths; (c) the cellular dislocation structure in the top part of the GIL; (d) the GIL at the depth of 200 μm under the surface. Note the increase of the laths size; (e) the GIL at the depth of 400 μm under the surface. Note the carbides and low density of dislocations.

The ordinary quenching has an appropriate soaking at a temperature above  $A_{c3}$ , the temperature of the ferrite-austenite transformation on heating, to allow phase transformation and homogeneous element distribution to take place.

The surface treatment by grinding entails the heating to above  $A_{c3}$  through the wheel-work material interaction to enable austenite phase to emerge. It brings about an absolute maximum temperature at the surface with a sharply decreasing gradient along the depth, making the GIL form in a non-uniform temperature field. In addition, the stress and strain rate in the grinding zone change and in turn affect the GIL formation. When the temperature rise is sufficient to make a ferrite-austenite transformation, the stress field brings about the deformation of austenite at a high strain rate so that cellular and polygonal dislocation structures are developed. The fast cooling of the top layer does not allow the structural relaxation of dislocations and thus martensite inherits

(Fig. 4c). The substructure generated in the austenite prevents the growth of martensite crystals and facilitates an increase in the number of nucleation centers. It causes the overall refinement of the martensite structure as shown in Fig. 4b.

In the deeper subsurface, say at the depth of  $200\ \mu\text{m}$  under the surface, the GIL structure is accomplished with a lower temperature rise and less deformation at a smaller strain rate. As a result, the dislocation density of the deformed austenite diminishes. Meanwhile, relaxation takes place, as the cooling time for this part of material is longer. The lower dislocation density in austenite results in larger martensite laths (Fig. 4d).

In the further deeper subsurface, at the depth of  $400\ \mu\text{m}$  under the surface for instance, the deformation in austenite becomes minor. In addition, the low cooling rate at this depth enables the formation of ferrite/bainite/martensite. Hence, both dislocations of low density and carbides appear (Fig. 4e).

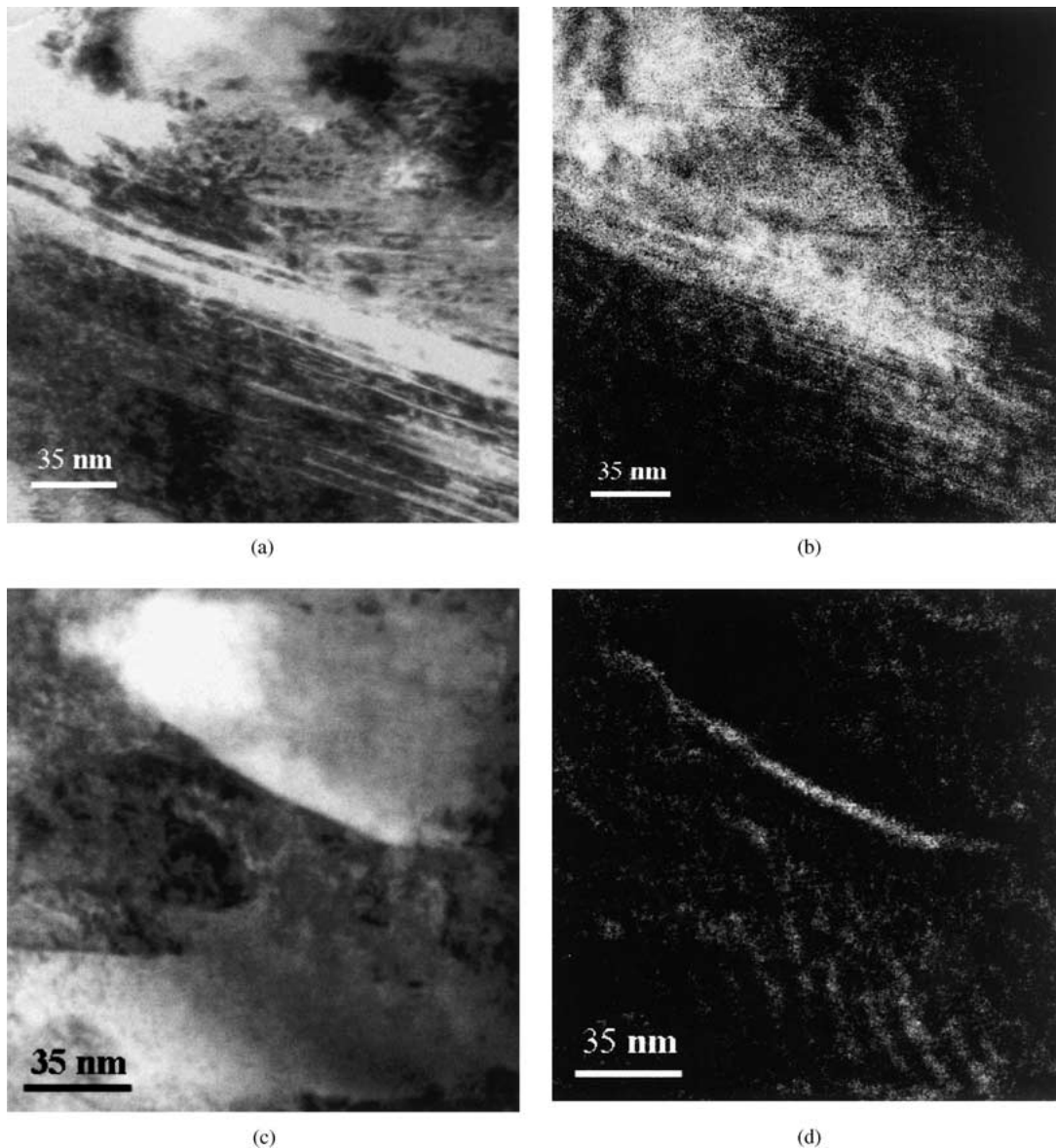


Figure 5 The electron micrograph of the top part of the GIL (Depth of cut =  $70\ \mu\text{m}$ , table velocity =  $0.1\ \text{m/min}$ ). (a) a general view; (b) the EELS carbon map. Note the additional concentration of carbon in the areas with twin martensite; (c) the boundary between two martensite laths; (d) the EELS carbon map at the lath boundary. Note the carbon segregation there; (e) the dislocation inside a martensite lath; (f) the EELS carbon map. Note a segregation of carbon at the dislocation; (g) a general view of the GIL at the depth of  $400\ \mu\text{m}$ ; (h) the EELS carbon map at this depth. Note the additional concentration of carbon in carbides. (Continued.)

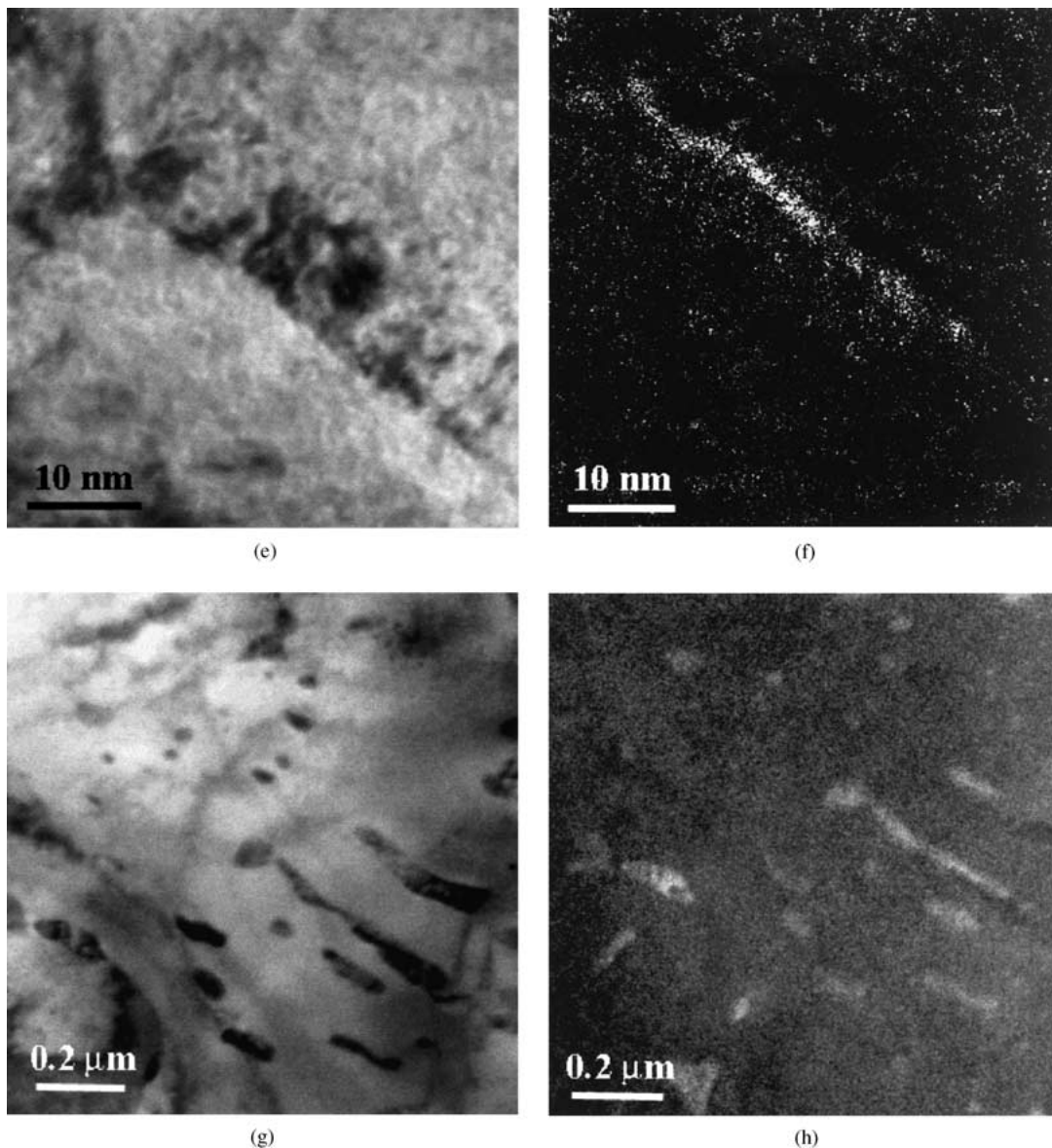


Figure 5 (Continued).

The above analysis shows that the formation of GIL is dependent on the temperature and stress fields generated by grinding. It follows that the GIL is governed by grinding variables and the structure formed is quite special, characterized by a very fine-grained martensite on the top sub-surface, a gradual growth of the grain-size along the subsurface depth, to a structure containing additional ferrite/bainite elements at the bottom. This structure promotes the beneficial mechanical properties of the GIL as to be discussed below.

#### 4.2. Wear

The wear rate of the GIL is two orders lower than that of the OM, as shown in Fig. 6a. For OM transition from mild to severe wear happens when the normal stress applied varies from 2 MPa to 3 MPa. At the stress of 5 MPa, adhesion takes place. However, GIL always exhibits mild wear in the whole process of wear testing. In addition, the friction coefficient with the specimens of OM is always higher.

The superior property of high wear resistance and low friction coefficient of the GIL is due to its spe-

cial microstructure. In the mild wear regime, it is easy to understand that GIL has a higher wear resistance because its hardness is much greater. In the severe wear regime, however, the wear resistance of a material depends largely on the stability of its microstructure [10, 11]. Both grain refinement and polygonal dislocation arrangement enhance the thermal and mechanical stability of the structure. Since the energy consumption for changing the GIL structure is higher, the GIL possesses a better wear resistance.

Inhomogeneous carbon distribution in GIL is undesirable from the point of view of improving wear resistance because it promotes the brittleness of martensite. However, since the dimension of martensite laths in GIL is significantly smaller compared with the OM, the actual carbon segregations over the lath boundaries in GIL are more evenly distributed and make the structure less brittle in comparison with OM.

Now consider the microstructural changes occurring during the wear tests. As can be seen in Fig. 7, an extensive precipitation of carbides takes place in both the OM and GIL. However, the size and distribution of the carbides are different. In OM, coarse plate-shaped

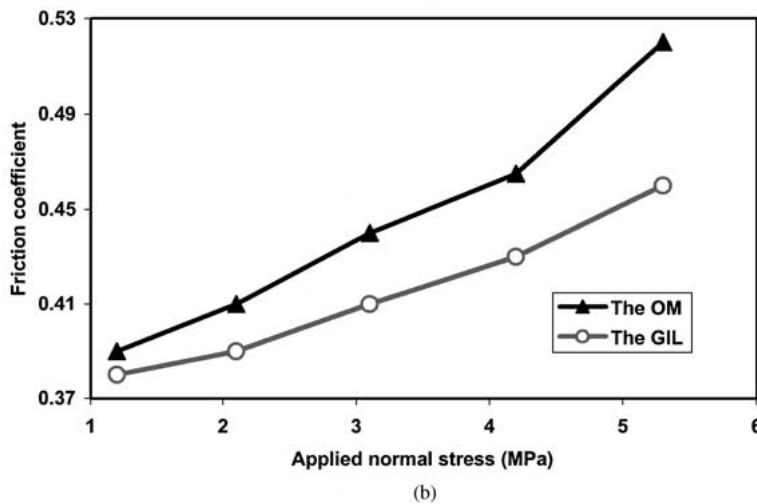
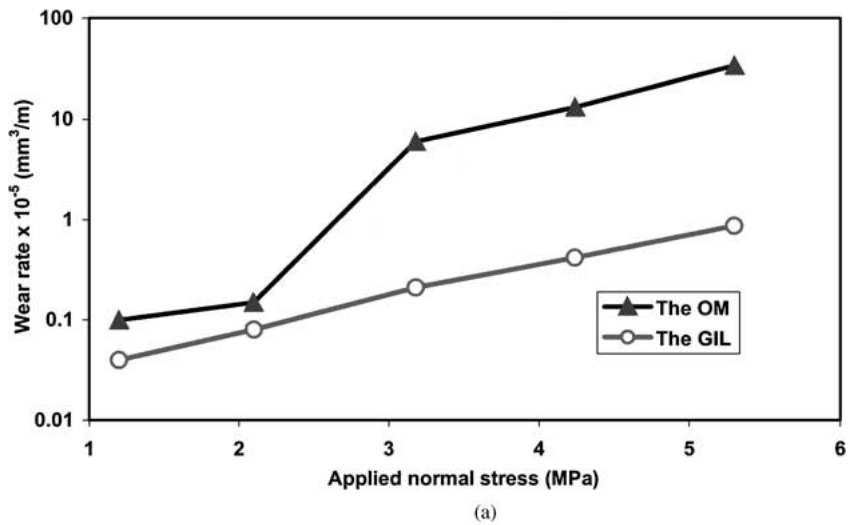


Figure 6 Wear and friction properties of OM and GIL. (a) wear rate; (b) friction coefficient.

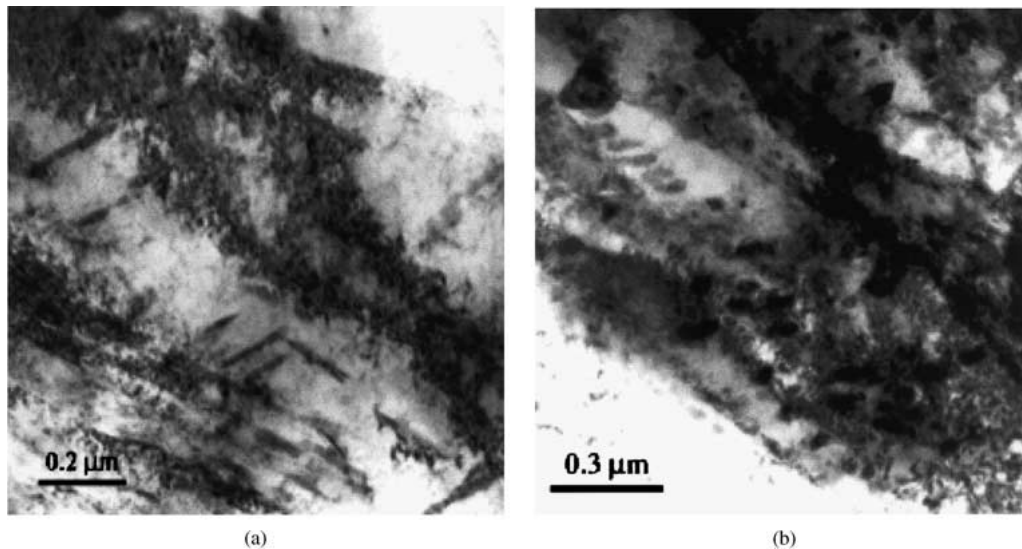


Figure 7 Subsurface structure after wear tests. (a) the OM; (b) the GIL.

carbides form throughout the laths. In GIL, however, carbides are more dispersed and appear mostly inside the laths. The two obvious factors that caused the difference are: (1) The refined martensite laths in the GIL make its total boundary length much longer and thus reduced the carbide concentration along the boundaries. (2) The cellular and polygonal distribution of disloca-

tions also promotes the carbide precipitation inside the martensite laths in GIL.

The precipitation of carbides during the wear tests increases the hardness of both OM and GIL, and thus improves their wear resistance. It is also advantageous from the point of view of structural changes because the formation of the tempered martensite increases the

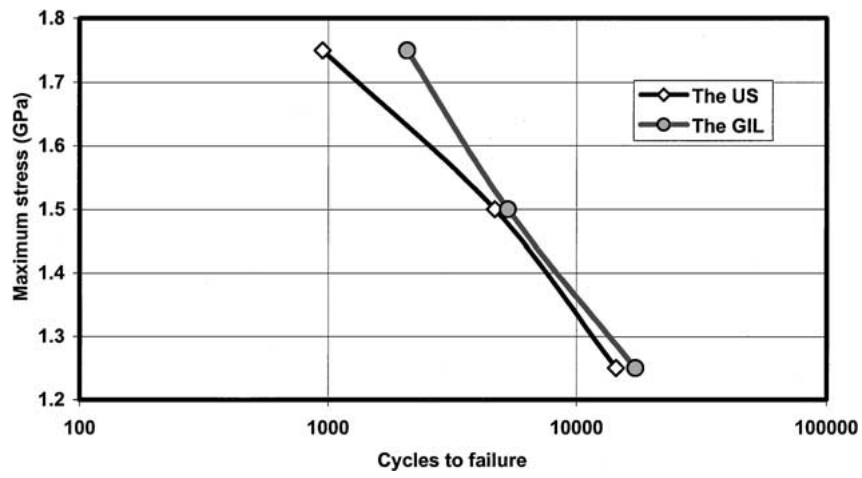
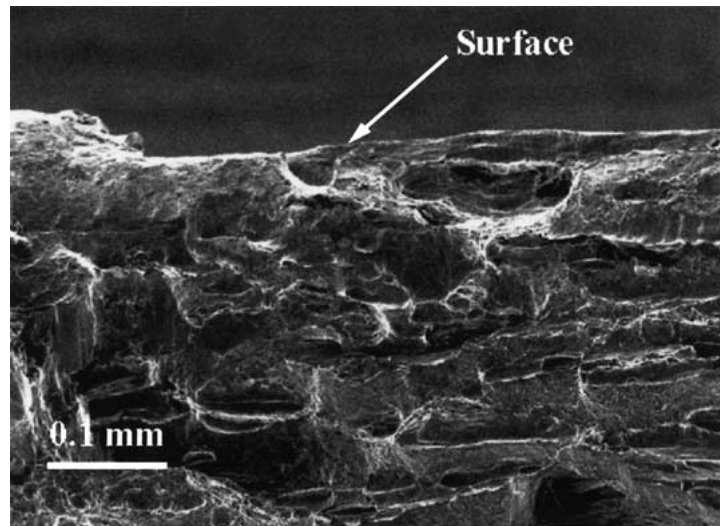
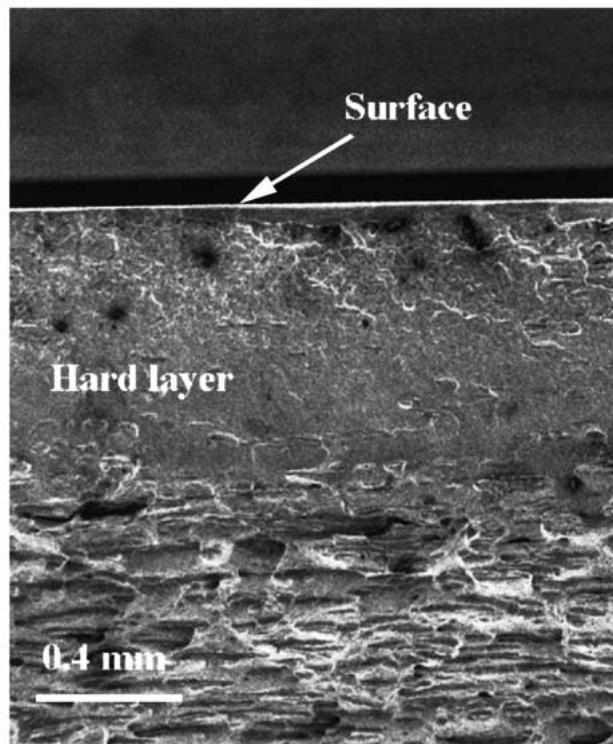


Figure 8 Fatigue life of OM and GIL.

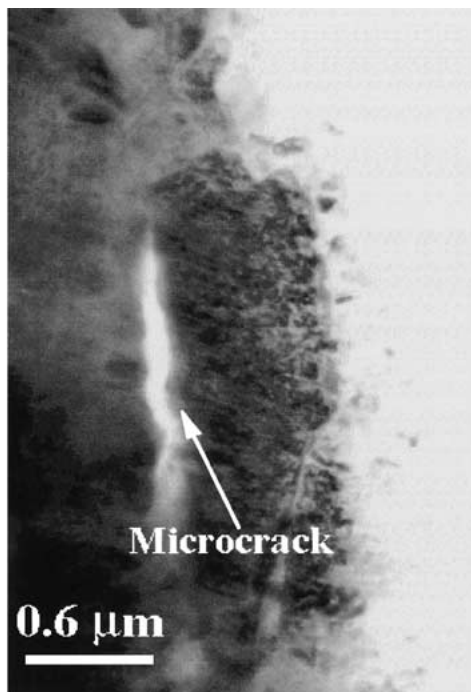


(a)

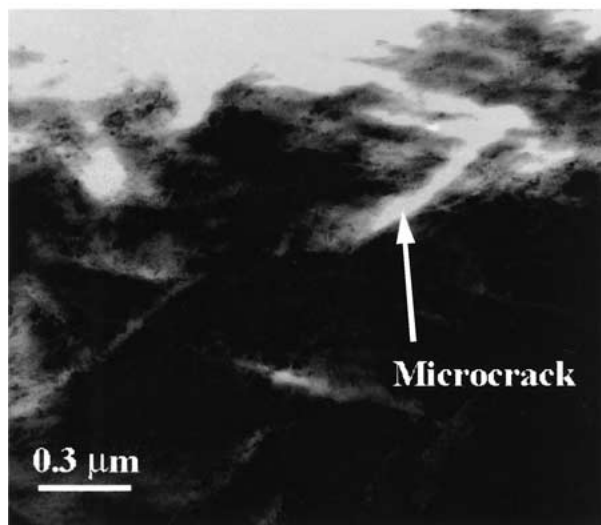


(b)

Figure 9 The surface topography. (a) to (b), and the electron structure, (c) to (d), of the samples after fatigue tests. (a) and (c) the US; (b) and (d) the GIL. (Continued.)



(c)



(d)

Figure 9 (Continued).

structural stability. However, more dispersed carbide precipitates in the GIL make the structure more uniform and thus leads to more improved wear properties.

Hence, both the original structure of the GIL and its changes during sliding wear are superior compared with the OM.

#### 4.3. Fatigue

Fig. 8 shows that GIL has a higher fatigue resistance. At the highest bending stress of 1.75 GPa in this study

the fatigue life of GIL is twice that of the untreated steel (US). At a lower bending stresses level, the improvement varies from 12% to 20%.

The topography of the fractured surfaces after fatigue experiments (Fig. 9) presents distinct characteristics of the GIL and US. The fractured surface of US (Fig. 9a) shows large brittle facets. The refinement of martensite structure in the GIL makes the facets much smaller (Fig. 9b). Since microcracks run mostly inside the martensite laths, as demonstrated by Figs 9c and d, networking of microcracks of individual martensite laths in the GIL is harder, because of its finer grains.

In addition, the high compressive residual stresses in GIL, which hinders the initiation and propagation of microcracks, play an important role in the improvement of GIL's fatigue life. A more detailed investigation about the residual stresses is still being undertaken in the authors' laboratory.

#### 5. Conclusions

The method of surface treatment by grinding leads to a grinding-induced layer, which has an advantageous microstructure and enhances the wear and fatigue properties of the ground components. Although the present study limits to one material, the mechanisms explored are applicable to a large class of quenchable steels whose heat treatment involves martensite phase transformation.

#### Acknowledgments

The authors wish to thank the Australian Research Council (ARC) for its continuing support of this project and the Electron Microscope Unit of Sydney University for using its facilities.

#### References

1. S. MALKIN, *Annals of the CIRP* **27** (1978) 233.
2. M. C. SHAW and A. VYAS, *ibid.* **43** (1994) 279.
3. E. IHALAINEN, *Acta Polyt. Scan., Mechanical Engineering Series* **1** (1981) 1.
4. L. ZHANG and M. MAHDI, *Int. J. Mach. Tools Manu.* **35** (1995) 1397.
5. M. MAHDI and L. ZHANG, *ibid.* **38** (1998) 1289.
6. *Idem.*, *ibid.* **39** (1999) 1285.
7. E. BRINKSMEIER and T. BROCKHOFF, *Annals of the CIRP* **45** (1996) 283.
8. T. BROCKHOFF, *ibid.* **48** (1999) 255.
9. S. MALKIN, "Grinding Technology. Theory and Applications of Machining with Abrasives" (Elis Horwood Ltd., Chichester, 1989).
10. Y. WANG, T. LEI and J. LIU, *Wear* **231** (1999) 20.
11. M. L. BERNSTEIN, L. M. KAPUTKINA, E. V. KONYUKOVA, N. A. NIKISHOV and R. N. SHAKHKERIMOV, *Rus. Met.* **1** (1985) 80.

Received 16 July 2001

and accepted 24 April 2002